Computers and Concrete, *Vol. 23, No. 5 (2019) 335-349*
DOI: https://doi.org/10.12989/cac.2019.23.5.335

Experimental study on shear damage and lateral stiffness of transfer column in SRC-RC hybrid structure

Kai Wu[*1,2], Jiangpeng Zhai[1a], Jianyang Xue[3b], Fangyuan Xu[1c] and Hongtie Zhao[3d]

[1]*College of Civil and Transportation Engineering, Hohai University, No. 1 Xikang Road, Gulou District, Nanjing city, PR China*
[2]*Department of Civil and Environmental Engineering, National University of Singapore, 21 Lower Kent Ridge Road, Singapore*
[3]*School of Civil Engineering, Xi'an University of Architecture & Technology, No. 13 Yanta Road Middle Section, Beilin District, Xi'an City, PR China*

(Received January 12, 2019, Revised April 10, 2019, Accepted April 13, 2019)

Abstract. A low-cycle loading experiment of 16 transfer column specimens was conducted to study the influence of parameters, likes the extension length of shape steel, the ratio of shape steel, the axial compression ratio and the volumetric ratio of stirrups, on the shear distribution between steel and concrete, the concrete damage state and the degradation of lateral stiffness. Shear force of shape steel reacted at the core area of concrete section and led to tension effect which accelerated the damage of concrete. At the same time, the damage of concrete diminished its shear capacity and resulted in the shear enlargement of shape steel. The interplay between concrete damage and shear force of shape steel ultimately made for the failures of transfer columns. With the increase of extension length, the lateral stiffness first increases and then decreases, but the stiffness degradation gets faster; With the increase of steel ratio, the lateral stiffness remains the same, but the degradation gets faster; With the increase of the axial compression ratio, the lateral stiffness increases, and the degradation is more significant. Using more stirrups can effectively restrain the development of cracks and increase the lateral stiffness at the yielding point. Also, a formula for calculating the yielding lateral stiffness is obtained by a regression analysis of the test data.

Keywords: lateral stiffness; transfer column; SRC-RC hybrid structure; shear distribution; concrete damage

1. Introduction

1.1 Steel reinforced concrete structure

Steel reinforced concrete (SRC) structure is a composite structure formed by embedding shape steel in the traditional reinforced concrete (RC) structure (Tong *et al*. 2016). Since the two materials are working together and able to bring out the advantages of each other, SRC members usually have higher strength, ductility and overall mechanical performance than the RC members (Kato and Takahashi 2000, Yue *et al*. 2019, Du *et al*. 2013). Also, due to the high resistance to earthquakes, fire, and corrosion, SRC member is widely used in the high-rise buildings, especially the high-rise buildings and skyscrapers in the earthquake regions (Han *et al*. 2016). The most significant shortcoming of SRC is the expensive cost. Recent years, researchers have made some progress in the optimal design of SRC structures. Narayan and Venkataramana (2007) studied the shape optimization of SRC beams and found that trapezoidal beams happened to be less costly than their rectangular counterparts. Zheng *et al*. (2011) studied the failure modes-based multi-objective optimal design of SRC frame structures.

1.2 SRC-RC vertical hybrid structure

SRC-RC vertical hybrid structure refers to a special transfer structure that uses the SRC columns in the lower floors and uses RC columns in the upper floors, which essentially is a vertically irregular structure. Currently, there are two main ways for the earthquake resistance design of the transfer floor between the SRC and RC columns: the middle height transfer method and the whole floor transfer method, as shown in Fig. 1. The middle height transfer method is widely applied in the Japanese design practice, which basically extends the shape steel from the SRC column up to a certain height and forms a special SRC-RC transfer column in the transfer floor. This method can reduce the sudden change in the stiffness and strength, avoid the "weak floor" during the earthquake.

SRC-RC vertical hybrid structure uses the high earthquake resistance from the lower SRC floors to enhance the seismic performance, also uses the upper RC floors to reduce the total cost. Therefore, it is widely used in engineering design due to the high earthquake resistance and relatively low cost.

During the Great Hanshin earthquake, Japan, however,

∗Corresponding author, Associate Professor
E-mail: wukai19811240@163.com
[a]Ph.D. Student
E-mail: zjp199506@163.com
[b]Professor
E-mail: jianyang_xue@163.com
[c]Ph.D. Student
E-mail: xfy_holiday@163.com
[c]Professor
E-mail: zhaohongtie@hotmail.com

ISSN: 1598-8198 (Print), 1598-818X (Online)

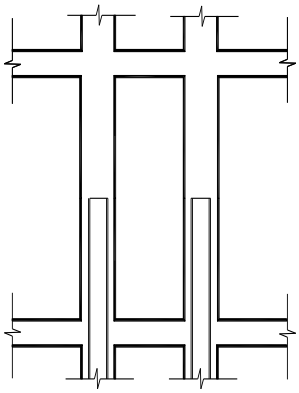

(a) Middle height transfer method

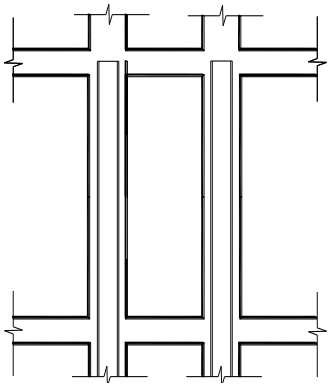

(b) Whole floor transfer method

Fig. 1 Design methods of the transfer floor

Fig. 2 Seismic damage of SRC-RC hybrid structures

the SRC-RC vertical hybrid structure was severely damaged, especially the transfer floor, as shown in Fig. 2, since there was no proper design method to consider the sudden change in stiffness at the transfer floor. So, some researchers studied the mechanical properties of the transfer column. Kimura and Shingu (1998) studied the influences of steel extension height and dense stirrups on the seismic performance of transfer columns. Kimura and Shingu (1999) further proposed a method that increases the longitudinal rebars to effectively achieve a smooth transfer. Kon-No *et al*. (1998), Imaizumi *et al*. (1998), Sugiyama *et al*. (1998) and Yamamoto *et al*. (2000) found out applying certain structural measures can enhance the seismic performance of transfer columns. Okamato *et al*. (1999) studied the influence of embedding length of shape steel on the mechanical properties of transfer columns. Suzuki *et al*. (1999a, 2000) found out the capacity of transfer column reduced with the increase of the extension length. Wu *et al*. (2011, 2016) studied the influence of extension length on the seismic performance of SRC-RC transfer columns under a low cyclic loading test of 16 transfer columns compared with 1 RC column, and analyzed the seismic behavior by the failure modes, hysteretic and skeleton curves, bearing capacity, deformation ability, stiffness degradation and energy dissipation. Gu *et al*. (2015) established the models of SRC-RC transfer column based on the fiber model and conducted a numerical analysis by the open source finite element software OpenSEES. The results showed that the axial compression ratio had a significant influence on the bearing capacity and hysteretic performance of the structure, while the stirrups ratio had less influence. Huang *et al*. (2017) investigated the shear capacity of SRC-RC transfer column and compared the experimental results with ABAQUS, considering different confinements for the concrete.

Overall, although some researchers have paid certain attention to the seismic performance and design method of SRC-RC vertical hybrid structure, they usually only focused on one or two design parameters and the specimen number is limited. There is still lacking more systematic researches on the seismic performance to propose a detailed calculation formula that can be used in the design practice.

1.3 Objective of this paper

After consulting a large number of relevant literatures on transfer columns, it is found that there is no systematic research and practical calculation formula on the lateral stiffness of transfer columns (Suzuki *et al*. 1999b, Yamaguchi *et al*. 2004), which highly delays the applications of SRC-RC vertical hybrid structure. This paper uses the extension length of shape steel, the ratio of shape steel, the axial compression ratio and the volumetric ratio of stirrups as parameters and conducts a low-cycle loading experiment of 16 transfer column specimens to study the shear distribution between steel and concrete and the acting height of the steel shear. We analyze the shear damage of concrete and the influences of those parameters on the lateral stiffness. Also, we propose a formula to calculate the lateral stiffness at the yielding point.

2. Experimental program

In this experiment, we design 16 transfer column specimens with a length L=1000 mm, shear span ratio λ=L /2h=2.5, and cross-section size of 220 mm×160 mm (h×b).

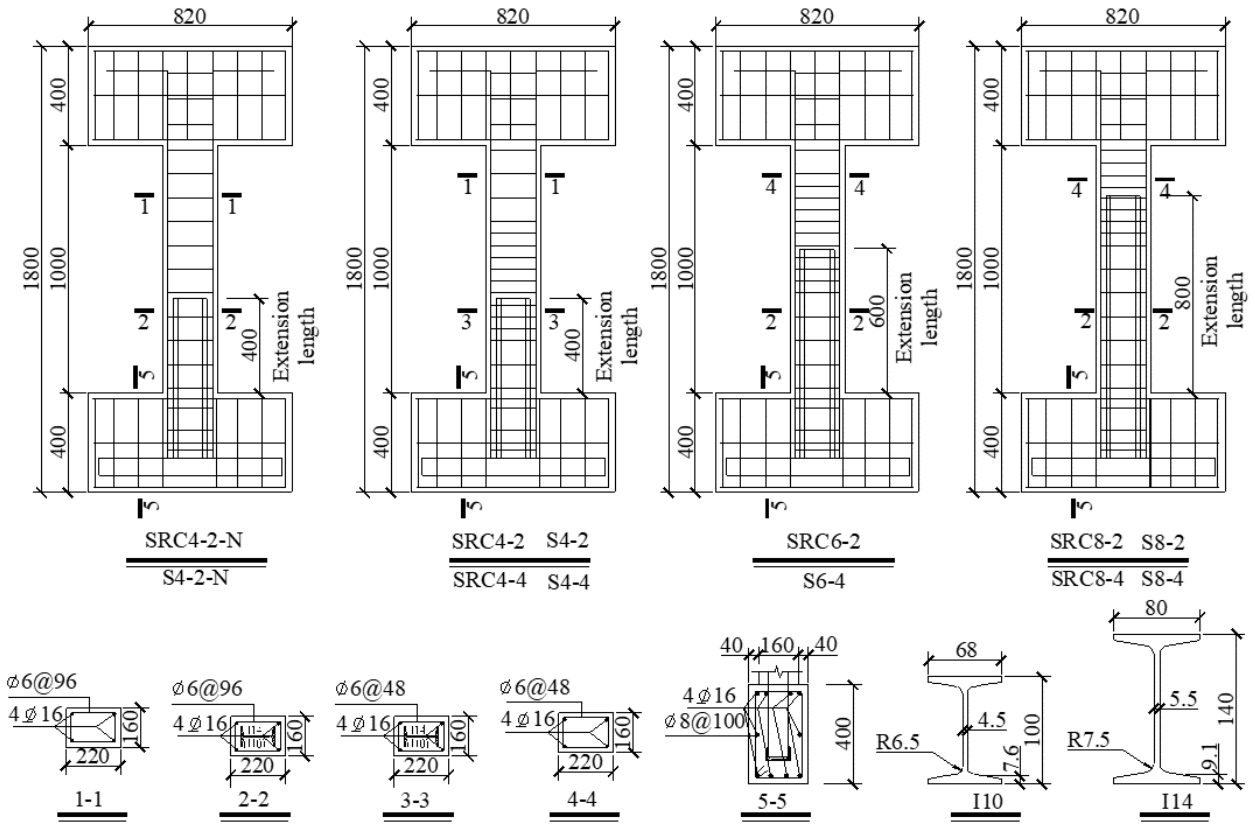

Fig. 3 Steel reinforcement arrangement and section dimensions of the shape steel (Measures in mm)

I10 and I14 shaped steel are used, which correspond to a steel ratio ρ_{ss} of 6.11% and 4.08%, respectively. The extension heights of the shape steel L_{ss} are 400 mm, 600 mm, and 800 mm, which correspond to an extending coefficient ξ ($\xi = L_{ss}/L$) of 0.4, 0.6 and 0.8, respectively. Use four 16 mm diameter rebars as longitudinal reinforcement and 6.5 mm diameter stirrups. Except for SRC4-2-N* and S4-2-N, other specimens all use dense stirrups. Some of them are only locally densified around the cutting regions of the shape steel, while others are fully densified along the whole column. The spacings for stirrups are 48mm and 96mm, which correspond to a volumetric ratio ρ_{sv} of 0.96% and 1.92%, respectively. The axial compression ratio n ($n=N/(f_c \cdot A)$) are 0.2 and 0.4, where f_c is the axial compressive strength of concrete, N is the axial compression and A is the section area. Fig. 3 shows the steel reinforcement arrangement for some specimens and the section dimensions of the shape steel I10 and I14. All specimens are cast with commercial concrete and the average compressive strength of 150 mm cubes is 59.1 MPa. According to code for design of concrete structures (GB 50010-2010), f_c=0.64×59.1 MPa =37.8 MPa. Use two batches of steel, and the measured mechanical properties are shown in Table 1.

Table 1 The measured mechanical properties of steel

Steel batch	Steel type	Model	f_y/MPa	f_u/MPa	E_s/MPa
First	Steel bar	ϕ6.5	364.3	461.5	2.01×10^5
		ϕ16	376.0	547.4	1.91×10^5
	Steel	I10 Flange	267.6	428.1	1.85×10^5
		I10 Webs	281.0	417.7	1.95×10^5
		I14 Flange	258.5	408.1	1.90×10^5
		I14 Webs	300.4	432.7	2.03×10^5
Second	Steel bar	ϕ6.5	383.6	507.1	1.95×10^5
		ϕ16	358.3	537.7	1.84×10^5
		ϕ20	356.7	558.5	1.68×10^5
		ϕ22	348.4	538.0	1.76×10^5
	Steel	I10 Flange	257.7	372.8	1.96×10^5
		I10 Webs	296.1	388.5	2.04×10^5
		I14 Flange	292.7	433.1	2.04×10^5
		I14 Webs	336.8	452.7	1.95×10^5

The loading device is shown in Fig. 4. Based on the preliminary studies and analysis, we estimated the yield loading and the ultimate loading of the specimens. The loading process is divided into two stages according to the estimated yield loading. Before the horizontal load reaching the yield loading, we use the loading control method, with an increment of 10 kN or 15 kN for each loading level. After reaching the yield loading, we use the displacement control method, with a displacement increment that equals to the yielding displacement for each displacement level. It is necessary to study not only the influence of displacement, but also that of cyclic Loading on seismic performance in this test. A large number of tests showed that before yielding load, the cyclic effect is negligible, so 1 cycle for each loading level is adopted (Kawashima and Koyama 1988, Pujol *et al.* 2006). After yielding load, the cyclic effect is often more significant, so 3 cycles for each displacement level are adopted.

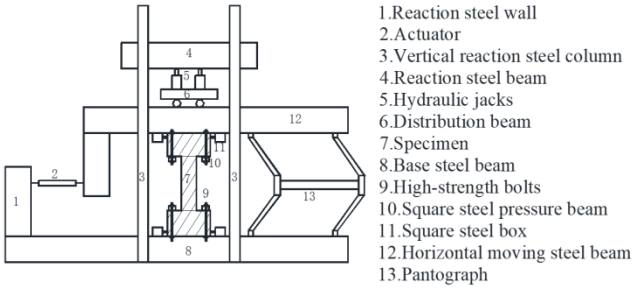

Fig. 4 Test set-up

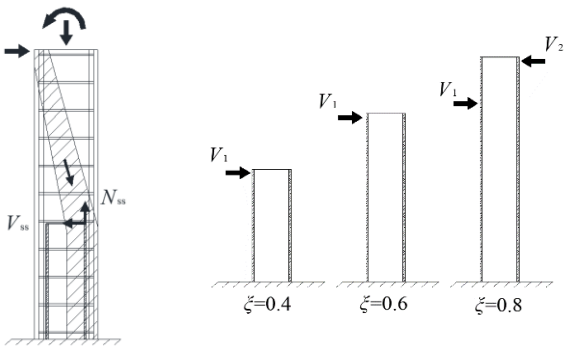

(a) Internal forces transfer (b) Steel shear for different ξ

Fig. 5 Interaction between shape steel and concrete

Table 2 shows the design parameters of the specimens and some experimental results. V is the ultimate shear capacity, V_{ss} is the steel shear force at the column base section under ultimate loading; L_v is the height of steel shear point, which is the distance from the steel shear point to the column base; The distribution coefficient of steel shear force is $\omega=V_{ss}/V$, which is the ratio between the steel shear force and the ultimate shear capacity of the specimen. The ductility coefficient μ reflects the deformation capacity of the specimens after yielding; η_m is the reduction factor of concrete under maximum loading, which reflects the damage state of concrete.

3. The shear distribution between steel and concrete

The shear span ratio reflects the relative size between the bending moment and shear force on the section. For frame columns, the shear span ratio affects the failure modes, the bearing capacity and also the lateral stiffness. When shear span ratio is large, the frame column is mainly under bending deformation, so it has high deformation capacity but relatively low lateral stiffness. When the shear span ratio decreases, the proportion of shear deformation for the frame column increases, so the deformation capacity is reduced while the lateral stiffness is improved. Therefore, the lateral stiffness increases with the decrease of shear span ratio for the frame column.

Because the shape steel only locally exists in the middle and lower part of the transfer column, the moment distributions between the bottom and top sections will change, and the inflection point will move up to the location about 0.6 of the column height. Within the column, concrete and steel interact in multiple ways to create an internal force transfer, which ensures the co-working and deformation compatibility between the two materials. As shown in Fig. 5, the relation between extension height and inflection point is the main influence factor of the mechanical properties between the concrete and shape steel.

When the extension height is lower than the inflection point, the horizontal component of the internal force between steel and concrete will act on the top part of the steel, along the same direction as the loading, denoted as V_1, and Steel shear $V_{ss}=V_1$, as shown in Fig. 5(a). When the extension height is higher than the inflection point, V_{ss} is composed of two parts, as shown in Fig. 5(b): the V_1; The second part is the horizontal force V_2 acting on the steel flange that is from the incompatible bending deformation between steel and concrete. The resulting force of V_1 and V_2

Table 2 Parameters of specimens and test data

Notation of specimens	ξ	n	Stirrups setting	Stirrups around the cut-off point of steel	V/kN	V_{ss}/kN	ω	L_v/L	μ	η_m	ρ_{ss} /%
SRC4-2-N*	0.4	0.2	ϕ6.5@96	-	124.0	85.9	0.69	0.28	1.97	0.119	6.11
S4-2-N	0.4	0.2	ϕ6.5@96	-	115.5	30.9	0.27	0.35	4.24	0.257	4.08
SRC4-2*	0.4	0.2	ϕ6.5@96	ϕ6.5@48	129.9	81.6	0.63	0.29	2.68	0.159	6.11
SRC4-4	0.4	0.4	ϕ6.5@96	ϕ6.5@48	152.3	92.2	0.61	0.23	2.75	0.175	6.11
S4-2*	0.4	0.2	ϕ6.5@96	ϕ6.5@48	125.2	32.8	0.26	0.33	3.28	0.264	4.08
S4-4	0.4	0.4	ϕ6.5@96	ϕ6.5@48	139.0	41.2	0.30	0.23	3.10	0.223	4.08
SRC6-2	0.6	0.2	ϕ6.5@96	ϕ6.5@48	127.7	47.6	0.37	0.50	3.78	0.451	6.11
S6-4	0.6	0.4	ϕ6.5@96	ϕ6.5@48	135.8	28.3	0.21	0.34	3.33	0.356	4.08
SRC8-2*	0.8	0.2	ϕ6.5@96	ϕ6.5@48	133.2	61.8	0.46	0.39	3.63	0.310	6.11
SRC8-4	0.8	0.4	ϕ6.5@96	ϕ6.5@48	146.3	69.5	0.48	0.30	3.54	0.296	6.11
S8-2*	0.8	0.2	ϕ6.5@96	ϕ6.5@48	115.1	27.2	0.24	0.40	3.85	0.303	4.08
S8-4	0.8	0.4	ϕ6.5@96	ϕ6.5@48	131.7	32.2	0.24	0.30	3.23	0.290	4.08
SRC4-2-JM*	0.4	0.2	ϕ6.5@48	-	134.7	86.3	0.64	0.28	4.65	0.150	6.11
SRC4-4-JM	0.4	0.4	ϕ6.5@48	-	147.4	86.5	0.59	0.24	3.39	0.189	6.11
S4-2-JM*	0.4	0.2	ϕ6.5@48	-	119.6	35.3	0.30	0.31	5.99	0.224	4.08
S4-4-JM	0.4	0.4	ϕ6.5@48	-	136.1	45.4	0.33	0.21	3.98	0.187	4.08


(a) Shear failure (S4-2*)


(b) Shear failure (S4-2-N)

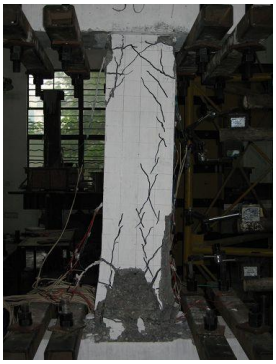
(c) Bending failure (S6-4)

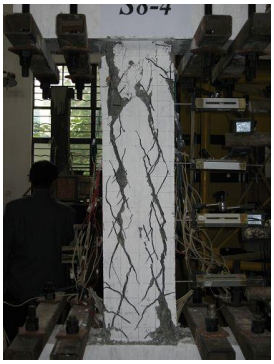
(d) Bond failure (S8-4)

Fig. 6 Failure modes of specimens

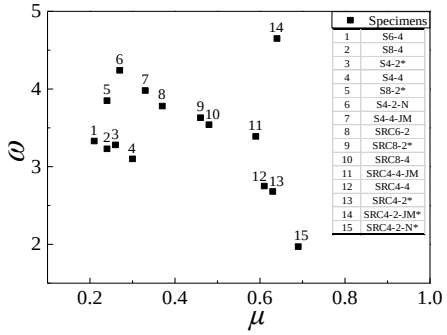

Fig. 7 Relation between ω and μ

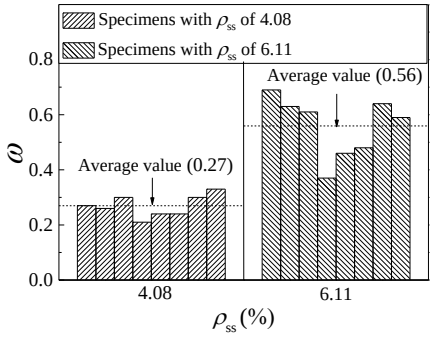

(a) Relation between ω and ρ_{ss}

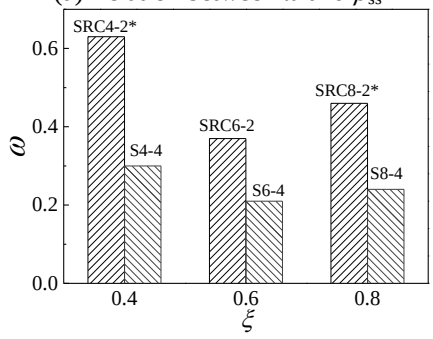

(b) Relation between ω and ξ

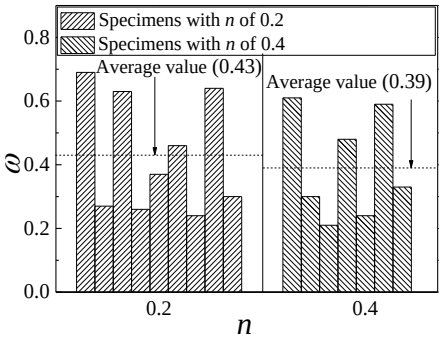

(c) Relation between ω and n

Fig. 8 Main influence factors of ω

acts on the steel and numerically equals the steel shear V_{ss} at the bottom of the shape steel. Its counter force acts on the concrete, equivalent to the lateral restraint of the concrete. This restraint changes the ratio between bending moment and shear force on the cross-section, resulting in the changes of actual shear span ratio of the specimens, also the changes in deformation capacity and lateral stiffness.

So, although the shear span ratio is 2.5, most specimens show a shear failure, and only a few go through the bond failure or bending failure. The shear failure usually occurs in the RC part that has a relatively lower shear capacity, while the bond failure and bending failure occur in the SRC part. Figs. 6(a)-(d) show the typical forms of failure. The interaction between steel and concrete and the resulting shear transfer are the primary reasons for this failure. Fig. 7 shows the relation between ω and μ. If more shear is resisted by the shape steel, the ductility and deformation capacity of the transfer column are usually lower.

As we can see from the collected data, the main influence factors of the shear distribution between steel and concrete are the steel ratio, steel extension height, and axial compression ratio. The stirrups ratio has a relatively small influence. The relations between ω and these main factors are shown in Fig. 8.

As shown in Fig. 8(a), ω increases with the ρ_{ss}. For specimens with larger ρ_{ss}, the bending capacity and bending stiffness of the steel are larger, so the steel web resists more shear force. As shown in Fig. 8(b), with the increase of ξ, ω first reduces and then increases and it reaches the minimum when ξ= 0.6. The change rate of ω relative to ξ is affected by ρ_{ss}, which is higher for a bigger ρ_{ss}. As shown in Fig. 8(c), with the increase of axial compression ratio n, ω has a certain decrease. For n= 0.2, ω is between 0.24 and 0.69, the average is 0.43; For n= 0.4, ω is between 0.21 and 0.61, the average is 0.39. Although a larger axial pressure will accelerate the elongation of bond cracks, it can delay the development of the shear cracks and bending cracks. Under

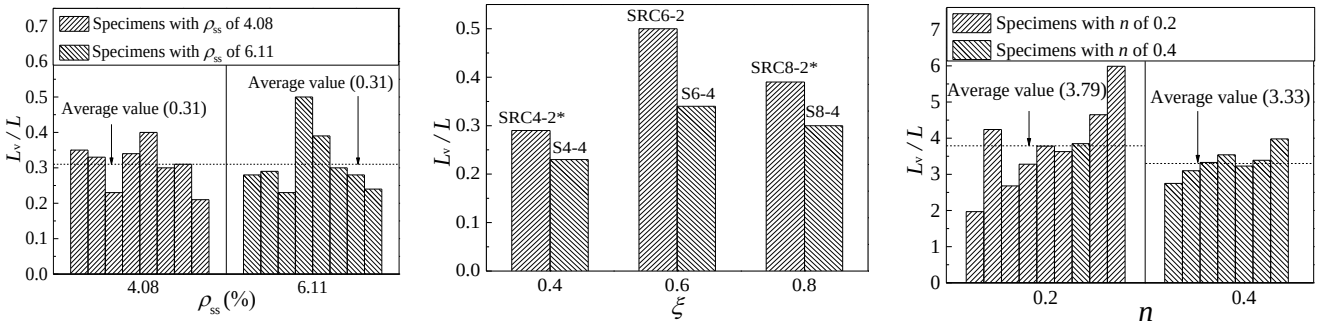

(a) Relation between L_v/L and ρ_{ss} (b) Relation between L_v/L and ξ (c) Relation between L_v/L and n

Fig. 9 Main influence factors of L_v/L

this condition the stiffness degradation of concrete is relatively slow, the bending moment and shear force on the concrete are big while the shear force resisted by the shape steel is small.

4. The acting height of the steel shear

The steel shear force is essentially the resulting force of the compressions between steel and concrete. When the extension height is lower than the inflection point, assuming the pressure is evenly distributed, then the steel shear point is at the middle of compression zone and the height of the compression zone is twice the distance from the steel shear point to the top of the shape steel. So L_v can also reflect the area of compression zone.

Fig. 9(a) shows the relation between ρ_{ss} and L_v/L. For specimens with I10 shaped steel, L_v/L is between 0.21 and 0.40, with an average of 0.31. For specimens with I14 shaped steel, L_v/L is between 0.23 and 0.50, with an average of 0.31. With the increase of ρ_{ss}, although the steel shear force increases, the width of the steel flange also increases, so the compression area within a unit height increases. Those two effects will cancel each other so that the ρ_{ss} eventually has little influence on L_v/L.

On the contrary of ω, L_v/L first increases and then reduces with the increase of ξ, as shown in Fig. 9(b). When ξ is less than 0.6, V_{ss} decreases with the increase of ω. The compression area between concrete and steel decreases, and the distance from the steel shear point to the top of the shape steel decreases, while the actual extension length increases, so L_v/L increases; When ξ is more than 0.6, the concrete and steel that are higher than the inflection points will create a compression force along the opposite direction of loading, which causes L_v/L to decrease gradually; ρ_{ss} also affects the change rate of L_v/L along with ξ. A higher ρ_{ss} is related to a higher change rate of L_v/L. When the steel of the bottom section reaches the yielding, L_v and V_{ss} are inversely proportional and V_{ss} can be calculated by the Eq. (1), where M_{ss} is the bending moment on the steel of the bottom section. So with the increase of ξ, the steel shear force should first reduce and then increase, which is exactly opposite with L_v.

$$V_{ss} = \frac{M_{ss}}{L_v} \tag{1}$$

Although the axial compression ratio n has a relatively small influence on ω, it shows an obvious influence on L_v/L. L_v/L decreases with the increase of n, as shown in Fig. 9(c). When n increases, the change of ω is not big, but because the bearing capacity of the specimen is greatly improved, the steel shear V_{ss} grows at the same time, the compression area increases, the distance from the steel shear point to the top of the shape steel increases, so L_v/L reduced accordingly.

5. The shear damage of concrete

The counter force of steel shear acts in the core concrete, creates tension and accelerates the damage. In the whole loading process, the shape steel and concrete have the same lateral displacement curve. Assume that the shape steel and concrete have the same curvature on the bottom section, and ignore the plastic deformation of steel, the shear distribution between two materials can be calculated with Eq. (2), where V_{ss} and V_c are the shear forces that resisted by the steel and concrete, respectively. The concrete damage reduction factor η can be calculated by Eq. (3), which is used to consider the damage of concrete under different shear loadings and the resulting reduction in bending stiffness of the concrete section.

$$\frac{V_{ss}}{V_c} = \frac{(EI)_{ss}}{\eta(EI)_c} \tag{2}$$

$$\eta = \frac{V_c(EI)_{ss}}{V_{ss}(EI)_c} \tag{3}$$

The η_m of 16 specimens in this experiment is between 0.12 and 0.45 and the difference in concrete damage is obvious. ρ_{ss}, ξ, n and many other factors all have an effect on the damage of concrete.

The correlation between ω and η_m is shown in Fig. 10(a), where we can find two rules: (1) the η_m of specimens with I14 shaped steel is less than the specimens with I10 shaped steel; (2) a bigger ω corresponds to a smaller η_m, and these two parameters have a linear correlation. Those two rules show the influence of steel shear force to the concrete damage: with the increase of ρ_{ss} and ω, the steel shear increases, and the indirect loading effect are more obvious at the concrete core area, so the concrete damage is more

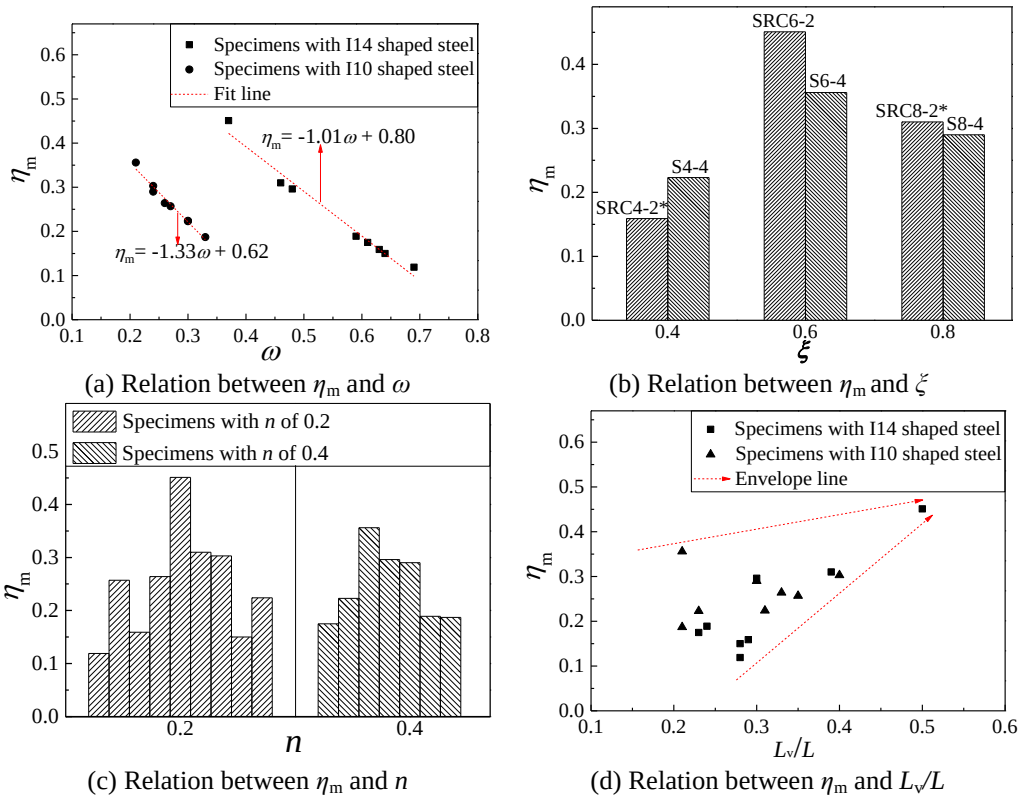

(a) Relation between η_m and ω (b) Relation between η_m and ξ

(c) Relation between η_m and n (d) Relation between η_m and L_v/L

Fig. 10 Main influence factors of η_m

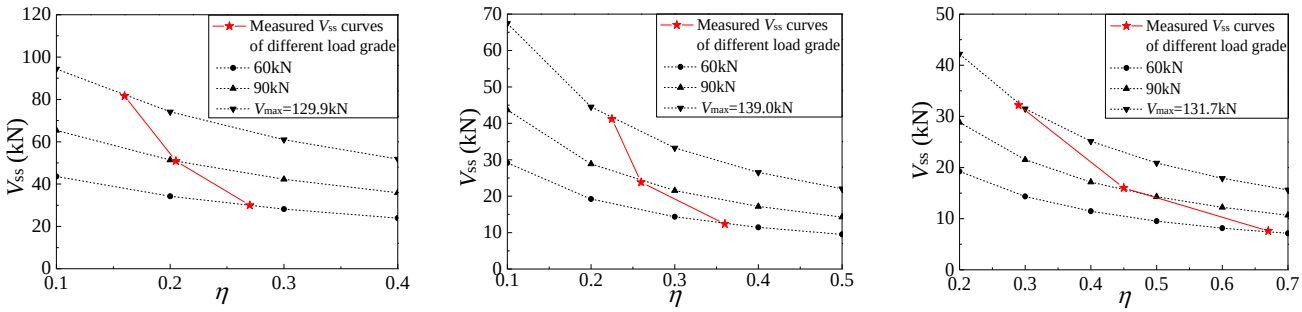

(a) SRC4-2* (b) S4-4 (c) S8-4

Fig. 11 Relation between V_{ss} and η

significant and η_m is smaller.

The correlation between ξ and η_m is shown in Fig. 10(b). With the increase of ξ, η_m first increases and then decreases, which is contrary to the patterns of ω. This pattern essentially reflects the influence of the steel shear force on the concrete damage. With the increase of ξ, the steel shear force first reduces and then increases, while η_m changes with an opposite pattern.

The correlation between axial compression ratio n and η_m is shown in Fig. 10(c). For specimens with the same n, the concrete damage shows a large variation with the change of the other factors. When n is big, the concrete has a strong crack resistance since the compression can delay the appearance and elongation of cracks, so the influence of other factors is relatively small and this variation in η_m is small.

The correlation between η_m and L_v/L is shown in Fig. 10(d). L_v reflects a comprehensive effect on η_m including the ρ_{ss}, n, L_{ss}, structural measures, and many other factors. With the increase of L_v/L, η_m shows a trend of increase. When the steel shear point is high, the concrete damage is relatively weak.

Fig. 11 shows the theoretical curve of η calculated from Eq. (3) and the one estimated from the test data. With the increase of loading, the steel shear gradually increases, the concrete damage gets more serious, η continually reduces, and the bending stiffness of the section decreases rapidly. Meanwhile, the concrete damage reduces the shear capacity of concrete even more, which leads to a further increase in steel shear. This continuous influence results in the accumulation of concrete damage until the specimen is unable to resist the loading and fails.

At the starting stage of loading, the concrete has good integrity and shares a large proportion of the shear. The concrete damage accumulates slowly, the area enclosed by the hysteretic curve is small and the energy dissipation from

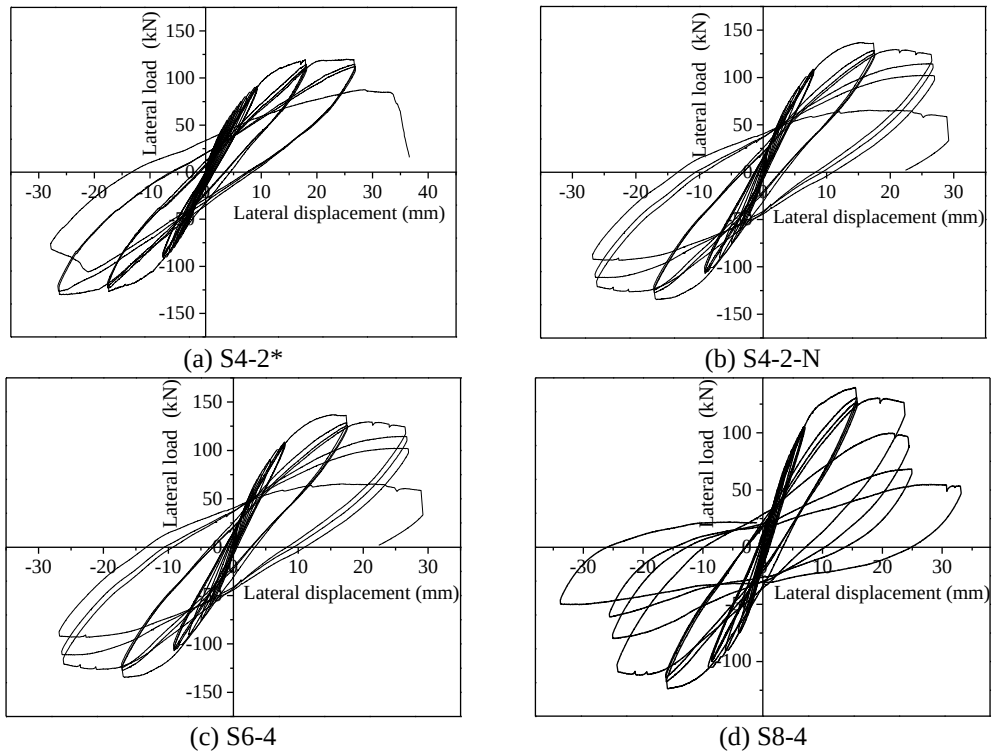

Fig. 12 Hysteretic curves of specimens

Table 3 Lateral stiffness of specimens

Notation of specimens	D_c/(kN/mm)			D_y/(kN/mm)			D_m/(kN/mm)		
	Push	Pull	Average value	Push	Pull	Average value	Push	Pull	Average value
SRC4-2-N*	14.58	23.81	19.20	9.19	10.64	9.91	7.01	6.56	6.78
S4-2-N	14.15	16.67	15.41	9.24	10.32	9.78	6.13	6.59	6.36
SRC4-2*	19.80	19.23	19.52	12.63	10.42	11.52	7.08	7.06	7.07
SRC4-4	26.60	25.25	25.92	16.20	17.08	16.64	10.77	8.59	9.68
S4-2*	17.24	18.69	17.97	10.25	11.77	11.01	4.75	5.03	4.89
S4-4	22.26	20.16	21.21	16.14	13.06	14.60	9.94	6.76	8.35
SRC6-2	14.71	14.14	14.42	10.75	10.08	10.41	5.45	4.18	4.81
S6-4	22.32	17.14	19.73	13.67	12.31	12.99	8.88	8.06	8.47
SRC8-2*	22.39	18.07	20.23	12.85	12.38	12.61	7.48	7.83	7.66
SRC8-4	23.08	22.46	22.77	16.24	16.55	16.39	9.73	9.63	9.68
S8-2*	20.71	17.86	19.28	12.18	10.68	11.43	7.69	4.69	6.19
S8-4	20.96	25.23	23.09	14.51	14.21	14.36	9.05	7.80	8.42
SRC4-2-JM*	19.77	19.70	19.74	11.28	11.01	11.14	6.36	6.86	6.61
SRC4-4-JM	18.10	21.83	19.97	11.84	13.70	12.77	5.31	7.08	6.19
S4-2-JM*	18.72	17.57	18.14	11.21	11.66	11.44	6.11	7.92	7.01
SRC4-2-N*	19.69	21.20	20.44	15.31	15.01	15.16	9.44	9.35	9.40
RC	18.07	21.74	19.91	8.73	12.52	10.63	4.24	6.82	5.53

concrete damage is limited. The hysteretic curves under cyclic loading are shown in Fig. 12. After yielding, there are many fully developed cracks in the specimen, and the nonlinear behavior gets more obvious. The area enclosed by the hysteretic curve and the energy dissipation from concrete damage both increase. Under maximum loading, the shape steel at the bottom of the column has yielded. Keep increasing the loading, the steel shear force remains the same, but the damage accumulation leads to a decrease of concrete capacity. Although lateral displacement at the top of the column continues to increase, the test loading begins to reduce. For specimens with large steel shear force, the capacity decreases more quickly because the concrete damage accumulates more rapidly. On the other hand, stirrups can restrain the elongation of concrete cracks, maintain the integrity of concrete, improve the ductility, deformation capacity and energy dissipation after the yielding.

After the yielding of specimens, the concrete cracks of some specimens are fully developed, resulting in the relative slips and the “pinch” phenomenon which indicates that the hysteretic curves of specimens are not plump any

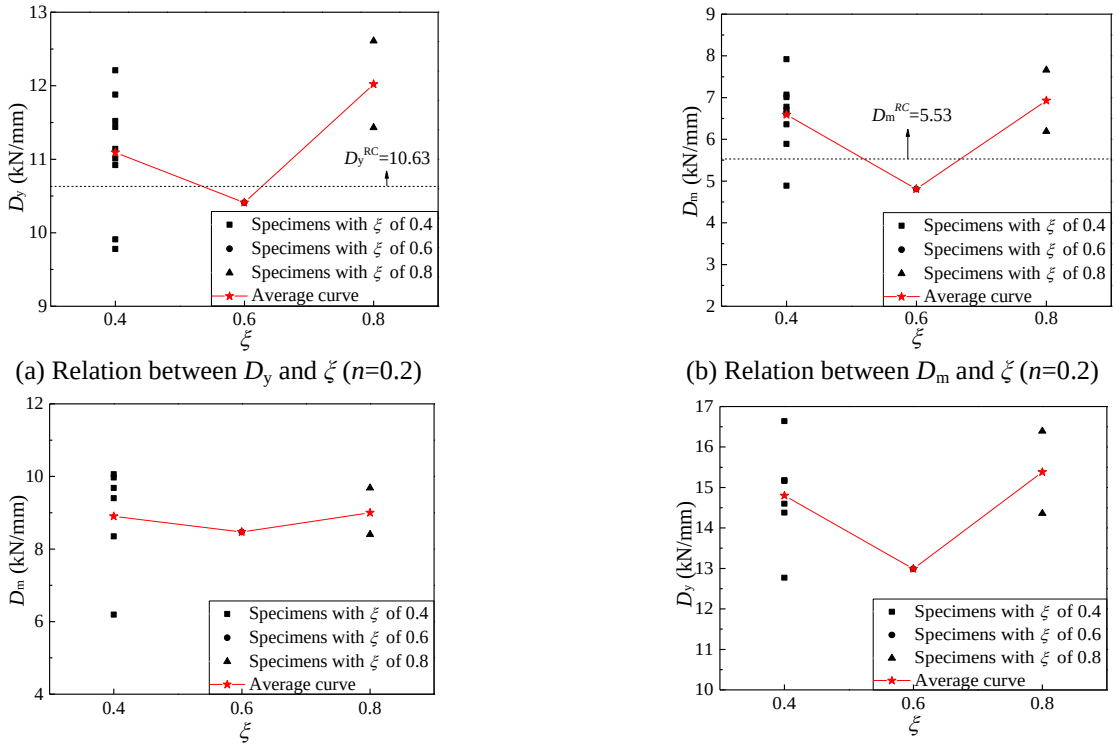

(a) Relation between D_y and ξ (n=0.2)

(b) Relation between D_m and ξ (n=0.2)

(c) Relation between D_y and ξ (n=0.4)

(d) Relation between D_m and ξ (n=0.4)

Fig. 13 Relation between D and ξ

longer in shapes. The area enclosed by the hysteretic curve decreases and the capacity under cyclic loading gets smaller. The relative slips that cause the "pinch" phenomenon mainly include the slip along bond cracks between steel and concrete, and the slip along the surface of fully developed shear cracks between concrete blocks.

6. The analysis of lateral stiffness

Fully understanding the influence factors of lateral stiffness and the stiffness degradation patterns under cyclic loading is important to the optimal design of SRC-RC vertical hybrid structure. The lateral stiffness corresponding to different characteristic displacement points under cyclic loading is calculated by the secant stiffness on the curve. Table 3 lists the lateral stiffness D_c that corresponds to the cracking loading, the lateral stiffness D_y that corresponds to the yielding loading, and the lateral stiffness D_m that corresponds to the maximum loading.

6.1 The influence factors of lateral stiffness

6.1.1 The extension length of shape steel

The extension length of shape steel is one of the main factors influencing the lateral stiffness of the transfer column. Fig. 13 shows the lateral stiffness of specimens with different extension lengths, where D_y^{RC} and D_m^{RC} are the lateral stiffnesses that correspond to the yield loading and the maximum loading of the RC specimen, respectively. With the increase of extension length, the lateral stiffness first drops then increases. When extension length is 0.6 of the column height, the lateral stiffness reaches the minimum.

According to Fig. 5, when the extension length is lower than the inflection point, V_1 is acting around the top of the shape steel, its value can be estimated by dividing the bending capacity of steel section with the extension length. Therefore, with the increase of extension length, V_1 decreases and the lateral restraint effect gets weaker, which means the lateral stiffness decreases. When the extension length is at the inflection point, V_1 reaches the minimum, the lateral restraint of specimens is the weakest, which means the lateral stiffness also reaches the minimum. If the extension length continues to increase, there will be a force V_2 between the steel and concrete, which will lower the acting point of the resultant steel shear. The steel shear and lateral stiffness both increase. Overall, with the increase of extension length, the actual shear span ratio increases first then decreases, while the lateral stiffness shows an opposite change pattern.

6.1.2 The ratio of shape steel

The steel ratio affects the lateral stiffness of transfer columns from the following two aspects: increasing the steel ratio can enhance the lateral support from the steel to the concrete, increase the horizontal force V_1 and the lateral stiffness; The shape steel and concrete compress each other and transfer the internal forces as the way shown in Fig. 14(a). The lateral restraint effect from shape steel acts on the core concrete, resulting in a horizontal tension in the section and the concrete is under a triaxial tension state, which will reduce the shear capacity and create a large number of shear cracks, so the lateral stiffness decreases. Fig. 14(b) shows the failure mode of the specimen with

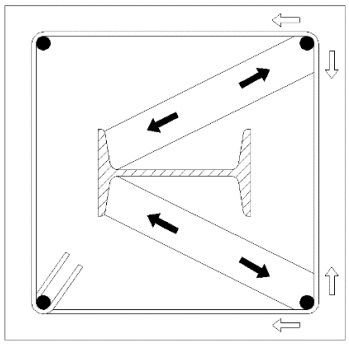

(a) Internal forces transmission

(b) Failure mode (SRC4-2-N*)

Fig. 14 Interaction and failure of transfer column

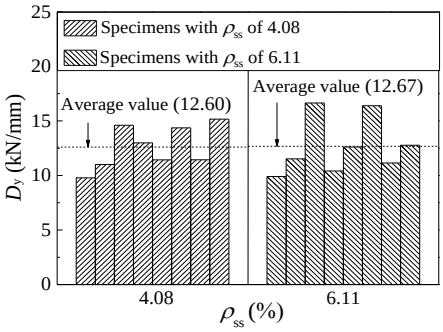

(a) Relation between D_y and ρ_{ss}

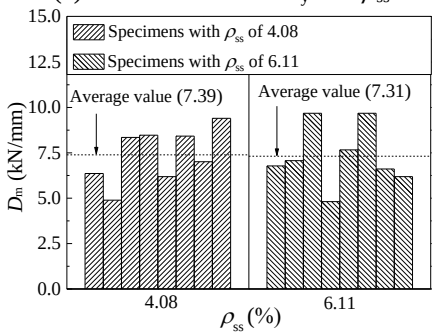

(b) Relation between D_m and ρ_{ss}

Fig. 15 Relation between D and ρ_{ss}

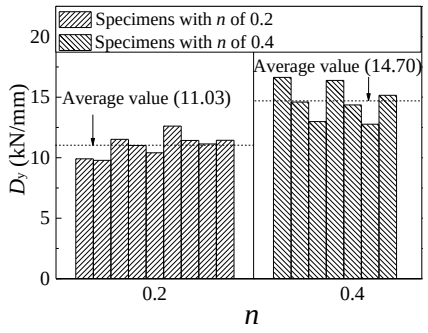

(a) Relation between D_y and n

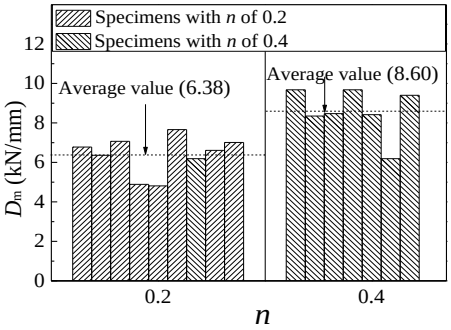

(b) Relation between D_m and n

Fig. 16 Relation between D and n

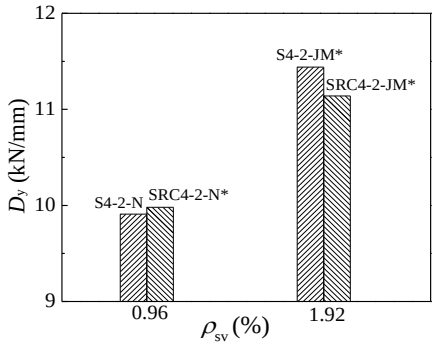

Fig. 17 Relation between D_y and ρ_{sv}

fewer stirrups. The tension within the core concrete creates a critical shear crack that cuts through the upper RC part of the specimen, which rapidly loses its capacity after this critical shear crack.

Fig. 15 shows the relation between the lateral stiffness and steel ratio for 16 transfer column specimens. With the increase of steel ratio, the lateral stiffness remains the same, which means the two aspects mentioned above basically counteract each other.

6.1.3 The axial compression ratio

The axial compression ratio is the main factor that affects the deformation ability of specimens. A large axial compression not only delays the appearance of cracks but also reduces the rotation of the cross section and plastic hinge, which means a bigger horizontal force is needed to have a unit lateral displacement. So the lateral stiffness increases with the axial compression ratio, as shown in Fig. 16. Under the yielding displacement, when the axial compression ratio increases from 0.2 to 0.4, the average lateral stiffness increases by about 33.6%. Under the displacement of maximum loading, the same increase of axial compression ratio leads to a 34.9% increase in the average stiffness.

6.1.4 The volumetric ratio of stirrups

The stirrup ratio also affects the lateral stiffness of specimens. Using more stirrups can reduce the concrete damage from internal tensions, effectively restrain the elongation of shear cracks and avoid the appearance of critical shear cracks. As shown in Fig. 17, increasing the stirrup ratio can improve the overall mechanical behavior of specimens and also the lateral stiffness.

6.2 The degradation of lateral stiffness

The degradation ratio k of lateral stiffness is defined as the ratio between the secant stiffness at the peak point of the

Table 4 Degradation ratio of specimens

Notation of specimens	k_1	k_2	k_3	k_4	k_5
SRC4-2-N*	0.98	0.57			
S4-2-N	0.96	0.96	0.95	0.71	
SRC4-2*	0.99	0.94			
SRC4-4	0.98	0.96	0.93		
S4-2*	0.97	0.95	0.78		
S4-4	0.99	0.95	0.93		
SRC6-2	0.99	0.96	0.96	0.96	
S6-4	0.97	0.93	0.79		
SRC8-2*	0.95	0.95	0.81	0.80	
SRC8-4	0.97	0.94	0.81		
S8-2*	0.95	0.95	0.91		
S8-4*	0.95	0.91	0.54		
SRC4-2-JM*	0.99	0.96	0.97	0.97	0.96
SRC4-4-JM	0.97	0.94	0.94		
S4-2-JM*	0.98	0.97	0.96	0.96	0.96
S4-4-JM	0.99	0.94	0.94	0.89	
RC	0.99	0.98	0.97		

first loading cycle and the secant stiffness at the peak point of the third loading cycle under certain displacement level. Overall, the lateral stiffness decreases with the number of cyclic loading, and the ratio k reflects the durability of specimens under cyclic loading. Table 4 shows the degradation ratio of each specimen, where k_i is the degradation ratio under the i-th displacement level.

The accumulated stiffness degradation coefficient w can be calculated by Eq. (4), which reflects the cumulative degradation of lateral stiffness under the whole loading process. A bigger w means the specimen has higher durability under cyclic loading and the lateral stiffness is more stable.

$$w_j = \prod_{i=1}^{j} k_i \tag{4}$$

Figs. 18-21 shows the degradation curves and accumulated degradation curves of some specimens with the increment of lateral displacement δ at the column top. In the degradation curve, D_0 is the secant stiffness at the peak point of the first loading cycle, which can be used as the elastic lateral stiffness. D is the secant stiffness at the peak point of a certain loading cycle, so D/D_0 can reflect the degradation of lateral stiffness. The extension length of shape steel, the ratio of shape steel, the volumetric ratio of stirrups and the axial compression ratio are the main factors that affect this degradation.

As shown in Fig. 18, the extension length has a direct influence on the stiffness degradation. The degradation gets faster with the increase of extension length, especially under high axial compression. The degradation is mainly related to the development of cracks. Fully developed cracks lead to significant degradation. When the extension length is big, there will be a large number of bond cracks between the steel and concrete. The close and reopen of bond cracks during the loading and the relative slip along the bond crack surface will cause the "pinch" phenomenon,

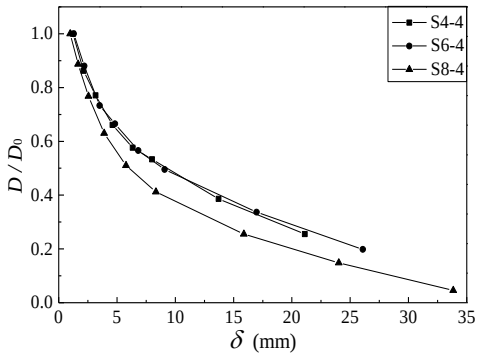

(a) Influence of ξ on D/D_0

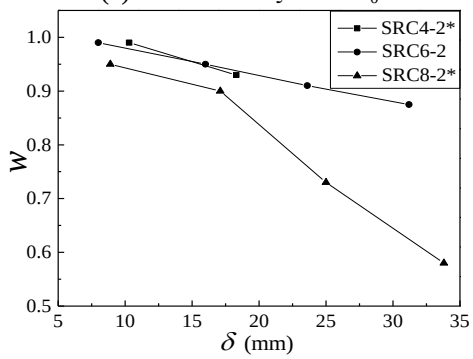

(b) Influence of ξ on w

Fig. 18 Influence of ξ on degradation of lateral stiffness

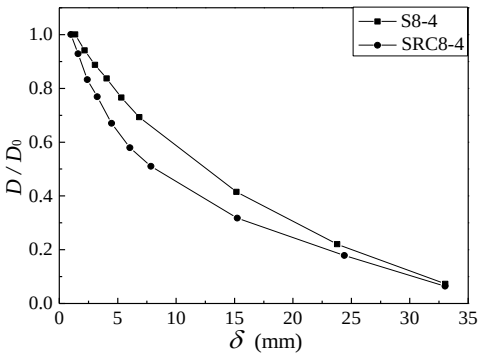

(a) Influence of ρ_{ss} on D/D_0

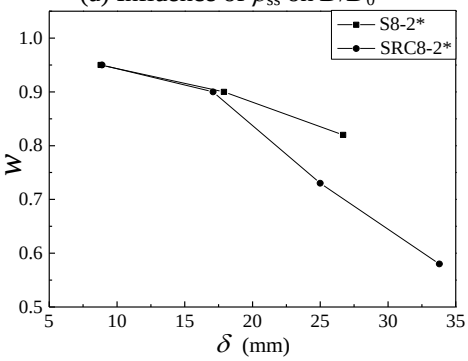

(b) Influence of ρ_{ss} on w

Fig. 19 Influence of ρ_{ss} on degradation of lateral stiffness

and also accelerate the stiffness degradation.

The steel ratio affects the degradation from the following two aspects: shape steels with a big cross-section area offer a larger lateral restraint to the concrete and enhance the shear effect, so the shear cracks can fully

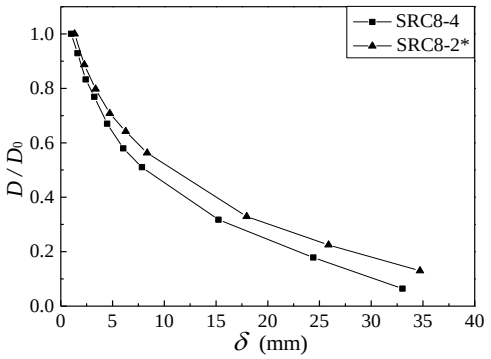

(a) Influence of n on D/D_0

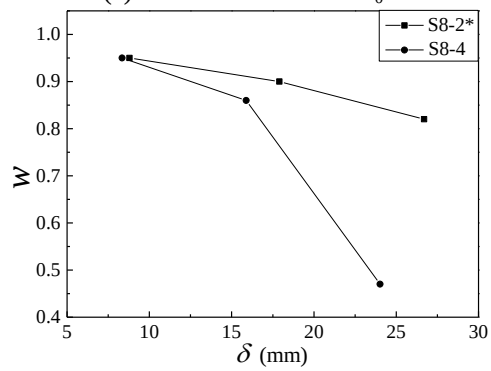

(b) Influence of n on w

Fig. 20 Influence of n on degradation of lateral stiffness

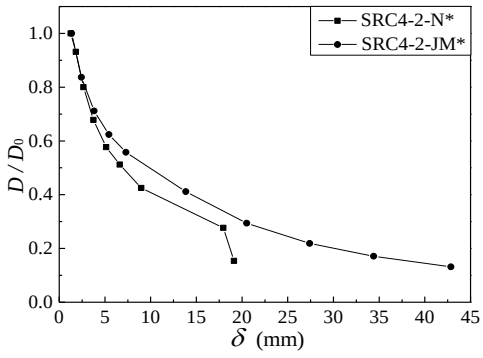

(a) Influence of ρ_{sv} on D/D_0

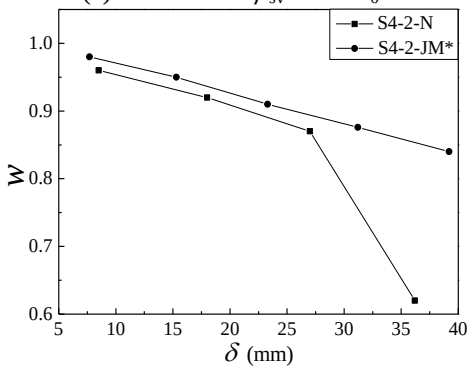

(b) Influence of ρ_{sv} on w

Fig. 21 Influence of ρ_{sv} on degradation of lateral stiffness

develop. On the other hand, the larger lateral restraint increases the horizontal tension on the section, reduces the mechanical performance of concrete and leads to more shear cracks and bond cracks. Therefore, the degradation rate increases with the steel ratio, as shown in Fig. 19.

A large axial compression ratio can increase the shear capacity of concrete, delay the appearance and development of shear and bending cracks, but it also speeds up the elongation of bond cracks, which leads to the increase of the degradation rate, as shown in Fig. 20.

The stirrups mainly affect the degradation by restraining the shear and bond cracks. So at the later stage of loading, the stiffness degradation of specimens with more stirrups is relatively slow, while at the beginning of loading, the influence of stirrups is small, as shown in Fig. 21.

7. The calculation of lateral stiffness

7.1 The elastic lateral stiffness

The loading method of this test can accurately simulate the loading condition of a frame column. The two ends can move in parallelly and the beam has a strong constraint on the column, so we can assume there is no rotation on both ends of the specimen and use the method of inflection point to calculate the elastic lateral stiffness.

Because the top and bottom sections of the transfer columns are different, we need to modify the common calculation formula. As shown in Fig. 22, when there is no rotation but there is displacement between two ends, the shear force and horizontal displacement of a transfer

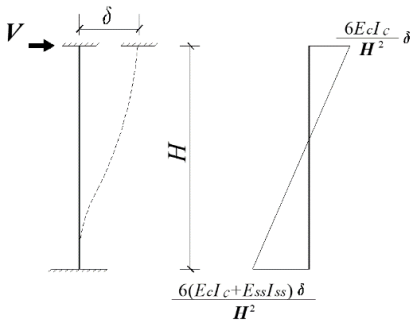

Fig. 22 Shear force and lateral displacement

column have the relation as shown in Eq. (5).

$$V = \frac{12E_cI_c + 6E_{ss}I_{ss}}{H^3}\delta \tag{5}$$

So the elastic lateral stiffness D can be calculated by Eq. (6). Because the extension length has a minor effect on the elastic lateral stiffness of transfer columns, it is not included in the formula.

$$D = \frac{V}{\delta} = \frac{12E_cI_c + 6E_{ss}I_{ss}}{H^3} \tag{6}$$

When the shear span ratio is small, we also need to consider the shear deformation. According to the mechanical model, the inflection point is at the middle height, so the shear deformation can be calculated with Eq. (7)

$$\delta_s = \frac{\alpha VH}{GA} \tag{7}$$

Table 5 Results of yielding lateral stiffness

Notation of specimens	Test result of D_y/(kN/mm)	Calculated result of D_y/(kN/mm)	Test result of D_y/ Calculated result of D_y
S4-2*	11.01	9.14	1.20
S4-2-N	9.78	9.14	1.07
S4-2-JM*	11.44	9.14	1.25
S4-4	14.6	14.32	1.02
S4-4-JM	15.16	14.32	1.06
S6-4	12.99	13.89	0.94
S8-2*	11.43	9.43	1.21
S8-4	14.36	14.85	0.97
SRC4-2-N*	9.91	12.52	0.79
SRC4-2*	11.52	12.52	0.92
SRC4-2-JM*	11.14	12.52	0.89
SRC4-4	16.64	15.98	1.04
SRC4-4-JM	12.77	15.98	0.80
SRC6-2	10.41	12.36	0.84
SRC8-2*	12.61	12.71	0.99
SRC8-4	16.39	16.33	1.00

where G is the shear modulus, and α is the correction factor due to the uneven distribution of shear stress on the cross-section, which can be calculated by Eq. (8).

$$\alpha = \frac{A}{I^2}\int_A \frac{S^2}{b^2}dA \tag{8}$$

where I is the moment of inertia, b is the section width at the shear point, S is the net moment of area about the neutral axis;

Eq. (9) is the formula for the elastic lateral stiffness of transfer columns after considering the shear deformation.

$$D = \frac{V}{\delta + \delta_s} = \frac{1}{\dfrac{H^3}{12E_cI_c + 6E_{ss}I_{ss}} + \dfrac{\alpha H}{GA}} \tag{9}$$

7.2 The lateral stiffness at yielding point

Under the yielding condition, bending cracks, shear cracks, and bond cracks have all appeared. So when calculating the lateral stiffness at yielding point D_y, we need to introduce the concrete stiffness reduction factor γ, which is used to consider the effect of cracks and the plastic deformation of concrete. When ignoring part of the shape steel is under plastic state and the shear deformation of the specimen, D_y can be calculated by Eq. (10).

$$D_y = \frac{12\gamma E_cI_c + 6E_{ss}I_{ss}}{H^3} \tag{10}$$

In order to simplify the calculation of γ, the following Eq. (11) only considers the three main influence factors: axial compression ratio, shape steel ratio and extension length.

$$\gamma = \frac{n\cdot\zeta}{25\rho_{ss}(1.9+n)} \tag{11}$$

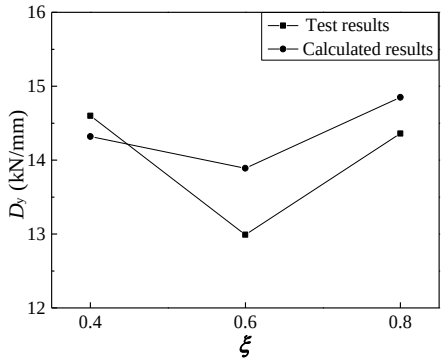

(a) n=0.4, ρ_{ss}=4.08%

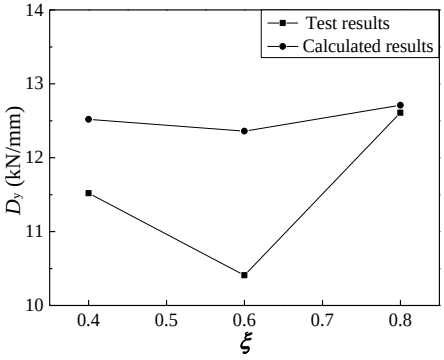

(b) n=0.2, ρ_{ss}=6.11%

Fig. 23 Test results and calculated results of yielding lateral stiffness

where ζ is a coefficient that accounts for the influence of extension length on γ, and by a regression analysis from the experimental data we get Eq. (12).

$$\zeta = 1.7\xi^2 - 1.9\xi + 1.6 \tag{12}$$

Table 5 lists the experimental value and theoretical value of the yielding lateral stiffness, as well as their ratio. The average value of this ratio is 1.000, while the mean square error is 0.139, which means the test results are very close to the theoretical results. Also, from Fig. 23, the test results and the theoretical results show a similar change pattern.

8. Conclusions

Conduct a low-cycle loading experiment of 16 transfer column specimens to study the concrete damage under cyclic loading, obtain the secant stiffness at displacements that corresponding to crack loading, yield loading, and maximum loading. We come with the following conclusions after analyzing the test data.

- The main influence factors of the shear distribution between shape steel and concrete include the steel ratio, the extension length of shape steel, and the axial compression ratio. The steel shear increases with the steel ratio; The steel shear first decreases then increases with the extension length, and it reaches the minimum when the extension length is 0.6 column height; The steel shear decreases with the axial compression ratio.

• The counter force of steel shear acts on the core concrete, creating the tensile stress, which accelerates the damage of concrete. The steel ratio, the extension length, the axial compression ratio, and many other factors affect the concrete damage. The bond slip and the shear slip of concrete reflect the influence of shear damage, lead to the "pinch" phenomenon and reduce the energy dissipation of the specimens. Meanwhile, the concrete damage reduces its shear capacity even more, which leads to a further increase in the steel shear. This continuous influence results in the accumulation of concrete damage until the specimen fails.

• With the increase of extension length, the lateral stiffness first decreases and then increases; With the increase of steel ratio, the lateral stiffness basically remains the same; With the increase of axial compression ratio, the lateral stiffness increases. Using more stirrups can effectively restrain the development of cracks and improve the yielding lateral stiffness.

• The degradation of lateral stiffness is influenced by the steel extension length, steel ratio, axial compression ratio, volumetric ratio of stirrups and many other factors. The extension length has a significant influence on the degradation rate, which gets faster with the increase of the steel extension length; For specimens with large steel ratio, the degradation of lateral stiffness is more severe; The stirrups mainly affect the degradation by restraining the shear and bond cracks. So at the later stage of loading, the stiffness degradation of specimens with more stirrups is relatively slow, while at the beginning of loading, the influence of stirrups is small; A large axial compression ratio can speed up the elongation of bond cracks, which leads to the increase of the degradation rate.

Acknowledgments

This work is supported by National Natural Science Foundation of China (Grant No.51208175) and the Fundamental Research Funds for the Central Universities (Grant No.2015B17514; 2016B20514).

References

Azizinamini, A. and Ghosh, S.K. (1997), "Steel reinforce concrete structures in 1995 Hyogoken-Nanbu earthquake", *J. Struct. Eng.*, **123**(8), 986-992. https://doi.org/10.1061/(ASCE)0733-9445(1997)123:8(986).

Dai, G.L., Jiang, Y.S., Fu, C.G. and Liang, S.T. (2003), "Experimental study on aseismic behaviors of transfer story with steel reinforced concrete in low stories of large space", *Chin. Civil Eng. J.*, **36**(4), 24-32.

Du, E.F., Shu, G.P. and Mao, X.Y. (2013), "Analytical behavior of eccentrically loaded concrete encased steel columns subjected to standard fire including cooling phase", *Int. J. Steel Struct.*, **13**(1), 129-140. https://doi.org/10.1007/s13296-013-1012-y.

GB 50010-2010 (2015), Code for Design of Concrete Structures, Ministry of Housing and Urban-Rural Development of the People's Republic of china; Beijing, China.

Gu, H., Zou, Y. and Chen, M. (2015) "Nonlinear numerical analysis of SRC-RC transfer columns based on OpenSEES", *Proceedings of the 3rd International Conference on Material, Mechanical and Manufacturing Engineering*, Guangzhou, China, June.

Han, L.H., Zhou, K., Tan, Q.H. and Song, T.Y. (2016), "Performance of steel-reinforced concrete column after exposure to fire: FEA model and experiments", *J. Struct. Eng.*, **142**(9), 1-13. https://doi.org/10.1061/(ASCE)ST.1943-541X.0001511.

Huang, W., Zhou, Z., and Liu, J.L. (2017), "Analytical deformation characteristics and shear capacity of SRC-RC transfer columns", *J. Constr. Steel Res.*, **138**, 692-700. https://doi.org/10.1016/j.jcsr.2017.08.024.

Imaizumi, T., Kon-No, S., Yamamoto, K. and Minami, K. (1998), "Experimental study on high-rise buildings with lower floor composed of SRC structure: part2 results and examination of experimentation", *Summaries of Technical Papers of Annual Meeting of Architectural Institute of Japan*, Kyushu, Japan, September.

Kato, T. and Takahashi, Y. (2000), "Earthquake design and construction of tall composite bridge piers", *Proceeding of the 12th World Conference on Earthquake engineering*, Auckland, New Zealand, January.

Kawashima, K. and Koyama, T. (1988), "Effect of number of loading cycles on dynamic characteristics of reinforced concrete bridge pier columns", *Struct. Eng. Earthq. E.*, **5**(1), 183-191. https://doi.org/10.2208/jscej.1988.392_205.

Kimura, J. and Shingu, Y. (1998), "Structural performance of SRC-RC mixed member under cyclic bending moment and shear", *Summaries of Technical Papers of Annual Meeting of Architectural Institute of Japan*, Kyushu, Japan, September.

Kimura, J. and Shingu, Y. (1999), "Structural performance of SRC-RC mixed member under cyclic bending moment and shear: effects of axial reinforcements inserted in SRC-RC joint", *Summaries of Technical Papers of Annual Meeting of Architectural Institute of Japan*, Kyushu, Japan, September.

Kon-No, S., Imaizumi, T., Yamamoto, K. and Ninami, K. (1998), "Experimental study on high-rise building with lower floor composed of SRC structure. Part1: Outline of the tests about deformation capacity of SRC columns", *Summaries of Technical Papers of Annual Meeting of Architectural Institute of Japan*, Kyushu, Japan, September.

Narayan, K.S.B. and Venkataramana, K. (2007), "Shape optimization of steel reinforced concrete beams", *Comput. Concrete*, **4**(4), 317-330. https://doi.org/10.12989/cac.2007.4.4.317.

Okamato, M., Baba, N. and Nishimura, Y. (1999), "Transfer from reinforced concrete members to steel reinforced concrete members (part 3)", *Summaries of Technical Papers of Annual Meeting of Architectural Institute of Japan*, Kyushu, Japan, September.

Pujol, S., Sozen, M.A. and Ramirez, J.A. (2006), "Displacement history effects on drift capacity of reinforced concrete columns", *ACI Struct. J.*, **103**(2), 253-262.

Sugiyama, K., Kon-No, S., and Yamamoto, K. and Minami, K. (1998), "Experimental study on high-rise buildings with lower floor composed of SRC structure: part3 outline of the tests about structural performance of column that is composed of SRC and RC, and test results of base experimentation", *Summaries of Technical Papers of Annual Meeting of Architectural Institute of Japan*, Kyushu, Japan, September.

Suzuki, H., Nishihara, H. and Matsuzaki, Y. (1999a), "Influence of steel existing the way of height of column on shear properties of RC column", *Proc. JPN Concrete Inst.*, **21**, 577-582.

Suzuki, H., Nishihara, H. and Matsuzaki, Y. (1999b), "Shear performance of the column where structural form changes from SRC to RC", *Summaries of Technical Papers of Annual Meeting*

of Architectural Institute of Japan, Kyushu, Japan, September.
Suzuki, H., Nishihara, H., Matsuzaki, Y. and Minami, K. (2000), "Structural performance of mixed member composed of steel reinforced concrete and reinforced concrete", *Proceedings of the 12th World Conference on Earthquake Engineering*, Auckland, New Zealand, January.
Tong, L.W., Liu, B., Xian, Q.J. and Zhao, X.L. (2016), "Experimental study on fatigue behavior of Steel Reinforced Concrete (SRC) beams", *Eng. Struct.*, **123**, 247-262. https://doi.org/10.1016/j.engstruct.2016.05.052
Wu, K., Xue, J.Y. and Zhao, H.T. (2011), "Experimental study on seismic performance of SRC-RC transfer columns and extension length of shape steel", *Proceedings of International Conference on Structures and Building Materials*, Guangzhou, China, January.
Wu, K., Xue, J.Y., Nan, Y. and Zhao, H.T. (2016), "Experimental research on seismic behavior of SRC-RC transfer columns", *Steel Compos. Struct.*, **21**(1), 157-175. https://doi.org/10.12989/scs.2016.21.1.157.
Yamaguchi, M., Kimura, J. and Chung, J. (2004), "Skeleton curve model of SRC-RC mixed columns", *Summaries of technical papers of Annual Meeting of Architectural Institute of Japan*, Tokyo, Japan, July.
Yamamoto, K.I., Komiya, Y., Kon-No, S., Imaizumi, T. and Sugiyama, K. (2000), "Experimental study on Seismic capacity composite column formed SRC and RC part", *Proceedings of the 12th World Conference on Earthquake Engineering*, Auckland, New Zealand, January.
Yang, Y., Guo, Z.X., Nie, J.G. and Zhao, H.T. (2005), "Study on seismic design of transmission story of SRC-RC vertical hybrid structures", *World Earthq. Eng.*, **21**(4), 60-65.
Yue, J.G., Qian, J. and Beskos, D.E. (2019), "Seismic damage performance levels for concrete encased steel columns using acoustic emission tests and finite element analysis", *Eng. Struct.*, **189**, 471-483. https://doi.org/10.1016/j.engstruct.2019.03.077.
Zheng, S.S., Li, Z.Q., Wang, B. and Li, L. (2011), "Failure modes-based multi-objective optimization design of steel reinforced concrete frame structures", *Key Eng. Mater.*, **450**(2), 219-222. https://doi.org/10.4028/www.scientific.net/KEM.450.219.

CC

Notations

L Height of specimens (mm)
λ Shear span ratio of specimens (-)
ρ_{ss} Ratio of shape steel (%)
L_{ss} Extension length of shape steel (mm)
ξ Coefficient of steel extension length (-)
ρ_{sv} Volumetric ratio of stirrups (%)
n Axial compression ratio (-)
f_c Axial compressive strength of concrete (MPa)
N Axial pressure (kN)
A Section area (mm^2)
V Ultimate shear capacity of specimens (kN)
V_{ss} Steel shear force at the column base section under ultimate loading (kN)
L_v Height of steel shear point (mm)
ω Distribution coefficient of steel shear force (-)
μ Ductility factor (-)
η_m Reduction factor of concrete under maximum loading (-)
f_y Yielding strength of steel (MPa)
f_u Ultimate strength of steel (MPa)
E_s Elastic modulus of steel (MPa)
V_1 Horizontal component of the internal force between the lower part of steel and concrete (kN)
φ_c Curvature of the concrete section (%)
φ_{ss} Curvature of the steel section (%)
V_2 Horizontal resulting force from the incompatible bending deformation between the upper part of steel and concrete (kN)
M_{ss} Steel moment at the bottom section of column (kN·mm)
V_{ss} Steel shear (kN)
V_c Concrete shear (kN)
η Reduction factor of concrete (-)
D_c Lateral stiffness corresponding to the cracking loading (kN/mm)
D_y Lateral stiffness corresponding to the yielding loading (kN/mm)
D_m Lateral stiffness corresponding to the maximum loading (kN/mm)
D_y^{RC} Lateral stiffnesses corresponding to the yield loading of the RC specimen (kN/mm)
D_m^{RC} Lateral stiffnesses corresponding to the maximum loading of the RC specimen (kN/mm)
K Lateral stiffness degradation ratio (-)
k_i Lateral stiffness degradation ratio under the i-th displacement level (-)
w Accumulated stiffness degradation coefficient (-)w_j
δ lateral displacement (mm)
D_0 Secant stiffness at the peak point of the first loading cycle (kN/mm)
D Secant stiffness at the peak point of a certain loading cycle (kN/mm)
G Shear modulus (MPa)
α Correction factor due to the uneven distribution of shear stress on the cross-section (-)
I Moment of inertia (mm^4)
b Section width at the shear point (mm)
S Net moment of area about the neutral axis (mm^3)
γ Concrete stiffness reduction factor (-)
ζ Coefficient accounting for the influence of extension length on γ (-)